Wave-number spectrum of electroencephalographic signals

S. C. O'Connor,[1,2,3] P. A. Robinson,[1,2,3] and A. K. I. Chiang[1,2]

[1]*Theoretical Physics Group, School of Physics, University of Sydney, New South Wales 2006, Australia*
[2]*Center for Wave Physics, School of Physics, University of Sydney, New South Wales 2006, Australia*
[3]*Brain Dynamics Center, Westmead Hospital and University of Sydney, Westmead, New South Wales 2145, Australia*

A recently developed, physiologically based continuum model of corticothalamic electrodynamics is used to derive the theoretical form of the electroencephalographic wave-number spectrum and its projection onto a one-dimensional recording array. The projected spectrum is found to consist of a plateau followed by regions of power-law decrease with various exponents, which are dependent on both model parameters and temporal frequency. The theoretical spectrum is compared with experimental results obtained in other studies, showing good agreement. The model provides a framework for understanding the nature of the spatial power spectrum by linking the underlying physiology with the large-scale dynamics of the brain.

I. INTRODUCTION

The electroencephalogram (EEG) is a noninvasive recording of the brain's electrical activity from electrodes on the scalp. The EEG frequency power spectrum has been widely investigated for a variety of brain states, such as the various states of arousal [1–3], during sensorimotor and mental tasks [3–5], and for both controls and patients afflicted with a number of brain disorders [6–10]. Consequently, there is a wealth of research into the features of these spectra. The investigation of spectral characteristics has permitted elucidation of many of the underlying physiological mechanisms responsible for their generation.

The spatial organization of brain function has been studied in animals and humans, in order to determine which regions of the cortex are involved in various cognitive and motor tasks [11–13]. Spatial correlations have been used to address the so-called binding problem, which poses the question of how spatially distant neurons correlate different aspects of a single stimulus [14,15]. Spatial coherence functions are also used to study cognition [3,16,17]. EEG has also been combined with magnetic resonance imaging to construct brain models [18]. These topographic studies of spatial EEG structure have wide diagnostic applications; however, the wave-number content of brain activity, the spatial analog of the frequency power spectrum, has received relatively little attention despite its potential to probe the spatial features of brain function from another perspective.

Research on the wave-number dependence of brain functions has been limited. It includes an early study of the frequency-wave-number domain [19], which investigated visually evoked response data in humans, using a spectral estimation technique which enabled the determination of the velocity of propagating wave fronts. Another early study investigated the wave-number spectrum near the alpha frequency, thereby providing evidence of a wave dispersion relation in the cortex [20]. More recent studies performed spatial spectral analysis of human electrocorticographic (ECoG) [21] and EEG [22–24] data.

Here we explore the wave-number spectrum using a recently developed neurophysical continuum model of cortical

dynamics. This model provides an established framework within which the neocortical wave-number content can be examined. It is a recently developed neurophysiological continuum model of corticothalamic activity [25–30] which incorporates distinct neural populations, nonlinearities, dendritic and axonal delays, and feedback to the cortex through the thalamus. It is able to reproduce many of the temporal characteristics of the EEG, such as the spectral peaks [26,30,31] and trends seen in various states of arousal [29], evoked response potentials [31], and certain seizure onsets and dynamics [32]. It has also addressed modal effects arising from cortical boundary conditions [30], and spatial coherence and correlations [33]. In the reverse direction, an individual's frequency power spectrum can be fitted to the model and the underlying physiological parameters deduced thereby [32,34].

One aim of this paper is to use the model to derive the wave-number power spectrum and to make predictions about its features for various states of arousal. We will investigate analytically the various spectral features and how in our model these relate mathematically and physiologically to the brain. A second aim is to compare the predicted spectra for various states of arousal with experimental data. We have chosen to use EEG data because the EEG is noninvasive and inexpensive, and so has more potential as a useful tool than the ECoG, which is obtained from the surface of the cortex during surgery.

In Sec. II of this paper our model is briefly outlined. The spatial spectrum is derived in Sec. III, and head volume conduction (which attenuates short wavelengths) is incorporated to allow comparison with scalp data. In Sec. IV, the derived spectrum and its parameter and frequency dependencies are explored. A comparison with experimental scalp data, for waking states with eyes closed and open, is detailed in Sec. V, and the form of a sleep-state spectrum is predicted. In Sec. VI, the choice of model parameters is discussed, and the values of previously ill-constrained parameters are estimated.

II. CORTICOTHALAMIC MODEL

In this section we summarize the corticothalamic model developed previously. The cortex is modeled as a two-

dimensional (2D) sheet, which is motivated by its relative thinness. In previous work [30] we examined the effects of boundary conditions on the cortical dynamics produced by this model, which contains both thalamocortical and cortico-cortical interactions, and found them to be minimal at most frequencies for systems of linear cortical sizes exceeding roughly 0.2 m, which is certainly satisfied for humans. The frequencies at which boundary conditions may still be important are where damping is the weakest, i.e., at $f \lesssim 1$ Hz, where there is a spectral enhancement, and near the alpha frequency (≈ 10 Hz) where boundary conditions may contribute to weak spectral substructure in our model. For most physiologically realistic parameters, however, the boundary conditions are not very important in determining the form of the spectrum produced by this model [30], in contrast to some other models in which the boundary conditions play a more critical role in determining dynamics because damping is intrinsically weak [24]. In our model, we have shown empirically that under most circumstances boundary conditions may be ignored [30]. We thus use the simplifying approximation that the cortex is infinite in extent. The probable effects of including boundary conditions into the spatial analysis of EEG signals presented here are discussed in Sec. VII.

The cortical model has randomly interconnected excitatory and inhibitory neurons. Scales below a few tenths of a millimeter are averaged over to yield a continuum treatment that extends from this scale to that of the whole cortex, as in other global models [24,35–38]. In our model, wave propagation through the cortex is governed by the mean firing rates (or *pulse densities*) of excitatory e and inhibitory i neurons. This mean neuronal firing rate has a sigmoidal dependence on cell-body potential, which we approximate here by a linear function on the assumption that deviations from the steady state are small at large scales in normal, nonseizure states. This approximation has been found to yield excellent agreement with observed frequency spectra [29].

The mean cell-body potential V_a of neurons of type a in the cortex is a function of inputs from other cortical neurons, and from excitatory subcortical neurons. Incoming activity is received in the dendritic tree and filtered as it travels along the dendrites to the cell body. Thus, the cell-body potential of a neuron of type $a = e, i$ can be written in Fourier space as

$$V_a(\mathbf{k}, \omega) = \sum_b L_a(\omega) G_{ab} \phi_b(\mathbf{k}, \omega), \qquad (1)$$

where $b = e, i, s$ and the G_{ab} are dimensionless gains representing the response strength in neurons a due to a unit signal incident from neurons of type b. The quantity L_a is a dendritic low-pass filter function, which accounts for the temporal delay and smearing of the incoming signal as it travels along the dendritic tree to the cell body. It can be written [25] as

$$L_a(\omega) = (1 - i\omega/\alpha)^{-1}(1 - i\omega/\beta)^{-1}, \qquad (2)$$

where β and α are the inverse rise and decay times of the dendritic potential.
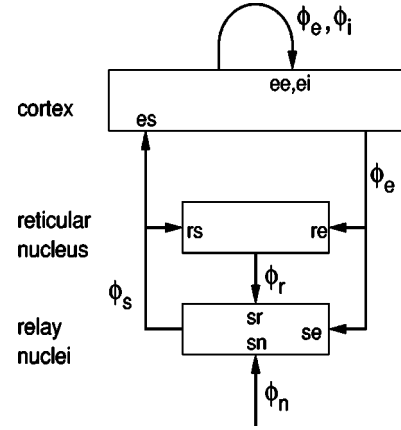
FIG. 1. Diagram of corticothalamic connections showing the cortex, reticular nucleus, and relay nuclei. The cortex is extensively connected to itself, and also projects to and receives projections from the thalamus. There are two loops through the thalamus: a direct loop passing only through the relay nuclei, and an indirect loop which also passes through the reticular nucleus. There is also an intrathalamic loop. Corticothalamic gains are indicated on the diagram.

The signal emitted by a single neuron depends on its cell-body potential. In the large-scale continuum treatment, we statistically average over scales below a few tenths of a millimeter to determine local mean values for quantities such as the cell-body potential and outgoing pulses. Thus we define a field of outgoing pulses in which the local mean value ϕ_a is determined by the local mean cell-body potential V_a, defined above. The propagating pulse density ϕ_a is then proportional to measured large-scale potentials, such as the EEG. This propagation can be described by damped wave equations for the fields ϕ_a [25]. In Fourier space one finds

$$D_a(\mathbf{k}, \omega) \phi_a(\mathbf{k}, \omega) = V_a(\mathbf{k}, \omega), \qquad (3)$$

where

$$D_a(\mathbf{k}, \omega) = k^2 r_a^2 + (1 - i\omega/\gamma_a)^2, \qquad (4)$$

$\gamma_a = v/r_a$ is a measure of the damping, v is the mean velocity of pulse propagation along an axonal tree, and r_a is the mean range of axons a.

Most subcortical signals ϕ_s arrive from the thalamus. The thalamocortical connectivity assumed in the model is shown in Fig. 1, involving the cortex, the thalamic relay nuclei, and the thalamic reticular nucleus. The (roughly 15) relay nuclei convey sensory information to relevant areas of the cortex [39]. These nuclei also receive signals from the cortex, which they topographically feed back to it. The thalamic reticular nucleus receives excitatory inputs from both thalamic relay and cortical neurons. Its output is inhibitory and acts solely on relay nuclei.

With reference to Fig. 1, we see that the subcortical input ϕ_s to the cortex is a filtered combination of subthalamic inputs ϕ_n and a feedback signal originating from ϕ_e in the cortex. If the time taken for a signal to travel from the cortex through the thalamus and back is t_0, we can write [31]

$$\phi_s(\mathbf{k},\omega) = P(\omega)\phi_n(\mathbf{k},\omega) + S(\omega)\phi_e(\mathbf{k},\omega), \tag{5}$$

where

$$P(\omega) = \frac{L_s G_{sn}}{1 - L_s G_{sr} L_r G_{rs}} e^{i\omega t_0/2}, \tag{6}$$

$$S(\omega) = \frac{L_s G_{sr} L_r G_{re} + L_s G_{se}}{1 - L_s G_{sr} L_r G_{rs}} e^{i\omega t_0}, \tag{7}$$

and ϕ_n is approximated as spatiotemporal white noise.

Incorporation of Eqs. (5)–(7) into Eq. (1), followed by the elimination of V_a from Eqs. (1) and (3), yields the transfer functions [31]

$$\frac{\phi_e(\mathbf{k},\omega)}{\phi_n(\mathbf{k},\omega)} = \frac{L_e G_{es} P}{1 - L_i G_{ii}} \frac{1}{k^2 r_e^2 + q^2 r_e^2}, \tag{8}$$

$$\frac{\phi_i(\mathbf{k},\omega)}{\phi_n(\mathbf{k},\omega)} = \frac{D_e L_i G_{is}}{D_i L_e G_{es}} \frac{\phi_e}{\phi_n}, \tag{9}$$

where

$$q^2 r_e^2 = (1 - i\omega/\gamma_e)^2 - \frac{L_e G_{ee} + L_e G_{es} S}{1 - L_i G_{ii}}. \tag{10}$$

III. WAVE-NUMBER SPECTRA

In this section we use the transfer functions (8) and (9) to derive the form of the wave-number power spectrum for both excitatory and inhibitory populations. In Sec. III B head volume conduction is incorporated to allow comparison with scalp data. Note that the spectra derived are 1D projections of the full 2D wave-vector spectrum, allowing comparison with data obtained from 1D electrode arrays.

A. The cortical spectrum

The power at a given $\mathbf{k}$ and ω is

$$P_a(\mathbf{k},\omega) = |\phi_a(\mathbf{k},\omega)|^2. \tag{11}$$

We integrate over one component of $\mathbf{k}$ to find the 1D wave-number spectrum for a fixed ω. For the excitatory population, this gives

$$P_e(k_x,\omega) = \int_{-\infty}^{\infty} |\phi_e(\mathbf{k},\omega)|^2 dk_y \tag{12}$$

$$= \frac{|\phi_N^2|}{r_e^4} \left| \frac{L_e G_{es} P}{1 - L_i G_{ii}} \right|^2 \int_{-\infty}^{\infty} \frac{dk_y}{|k^2 + q^2|^2} \tag{13}$$

$$= \frac{|\phi_N^2|}{r_e^4} \left| \frac{L_e G_{es} P}{1 - L_i G_{ii}} \right|^2 \frac{\pi}{2\,\mathrm{Re}[\sqrt{q^2 + k_x^2}]|q^2 + k_x^2|}. \tag{14}$$

Similarly, for the inhibitory population,

$$P_i(k_x,\omega) = \int_{-\infty}^{\infty} |\phi_i(\mathbf{k},\omega)|^2 dk_y \tag{15}$$

$$= \int_{-\infty}^{\infty} |\phi_e(\mathbf{k},\omega)|^2 \left| \frac{D_e L_i G_{is}}{D_i L_e G_{es}} \right|^2 dk_y \tag{16}$$

$$= \frac{|\phi_N^2|}{r_e^4} \left| \frac{L_e G_{es} P}{1 - L_i G_{ii}} \right|^2 \left| \frac{L_i G_{is}}{L_e G_{es}} \right|^2 \int_{-\infty}^{\infty} \left| \frac{D_e}{D_i} \right|^2 \frac{dk_y}{|k^2 + q^2|^2} \tag{17}$$

$$= \int_{-\infty}^{\infty} \frac{|k^2 r_e^2 + (1 - i\omega/\gamma_e)^2|^2}{|k^2 r_i^2 + (1 - i\omega/\gamma_i)^2|^2} \frac{|A(\omega)| dk_y}{|k^2 + q^2|^2}, \tag{18}$$

where

$$A(\omega) = \left(\frac{L_i G_{is} P \phi_N}{r_e^2 (1 - L_i G_{ii})} \right)^2. \tag{19}$$

We can write this as

$$P_i(k_x,\omega) = A_1 I_1 + A_2 I_2 + A_3 I_3, \tag{20}$$

where

$$A_1(\omega) = |A| r_e^4/r_i^4, \tag{21}$$

$$A_2(k_x,\omega) = 2|A|(1 - \omega^2/\gamma_e^2 + r_e^2 k_x^2)^2 r_e^2/r_i^4, \tag{22}$$

$$A_3(k_x,\omega) = |A|[r_e^4 k_x^4 + 2 r_e^2 k_x^2(1 - \omega^2/\gamma_e^2)$$

$$+ (1 + \omega^2/\gamma_e^2)^2]/r_i^4, \tag{23}$$

$$I_1(k_x,\omega) = \int_{-\infty}^{\infty} \frac{k_y^4 dk_y}{|k^2 + h^2|^2 |k^2 + q^2|^2}, \tag{24}$$

$$I_2(k_x,\omega) = \int_{-\infty}^{\infty} \frac{k_y^2 dk_y}{|k^2 + h^2|^2 |k^2 + q^2|^2}, \tag{25}$$

$$I_3(k_x,\omega) = \int_{-\infty}^{\infty} \frac{dk_y}{|k^2 + h^2|^2 |k^2 + q^2|^2}, \tag{26}$$

$$h = (1 - i\omega/\gamma_i)/r_i \approx 1/r_i. \tag{27}$$

The integrals (24)–(26) are evaluated in the Appendix.

B. The scalp spectrum

In order to allow comparison with scalp EEG data, we must incorporate spatial filtering of the signal by volume conduction in the cerebrospinal fluid, skull, and scalp. Srinivasan *et al.* have derived a scalp transfer function using a four-concentric-shell volume conductor model of the head [40], the four shells being the brain, cerebrospinal fluid, skull, and scalp. The function is calculated in the wave-number domain using a range of relative conductivities for the four shells. These results may be incorporated into our

model by introducing a volume conduction filter function that attenuates short-scale $(k>k_0)$ potential variations [24,29]. For many purposes the following are suitable approximate forms:

$$F(\mathbf{k}) = \frac{k_0^2}{k^2 + k_0^2} \tag{28}$$

or

$$F(\mathbf{k}) = e^{-k/k_0}. \tag{29}$$

Srinivasan *et al.* presented their results in a plot of the head transfer function T against the spherical harmonic degree [40]. The quantity T^2 is the filter function F in the present nomenclature, and the spherical harmonic degree can be converted to a wave number via the relation

$$k^2 = \frac{n(n+1)}{R^2}, \tag{30}$$

where n is the harmonic degree and $R = 0.8$ m is the radius of the head. Fits of Eqs. (28) and (29) to their model results yield values of $k_0 \approx 10–15$ m^{-1}. Additional uncertainties arise from the fact that Srinivasan *et al.* assumed a uniform spherical head with a skull of constant thickness. The effect on the spectrum of varying k_0 over the range 5 m$^{-1} < k_0 < 30$ m^{-1} is investigated in Sec. IV B. We find that a preliminary fit to data yields a value of k_0 which is consistent with the results of Srinivasan *et al.*

Using the filter function given in Eq. (28), the excitatory power is given by

$$P_e(k_x, \omega) = \int_{-\infty}^{\infty} |\phi_e(\mathbf{k}, \omega)|^2 F(\mathbf{k}) dk_y \tag{31}$$

$$= \frac{L_e G_{es}}{L_i G_{is}} |A| \frac{B k_0^2 \pi}{(c-d)(c-e)(d-e)}, \tag{32}$$

with

$$B(k_x, \omega) = \sqrt{\frac{1}{c}}(d-e) + \sqrt{\frac{1}{d}}(e-c) + \sqrt{\frac{1}{e}}(c-d), \tag{33}$$

$$c(k_x, \omega) = k_x^2 + q^2, \tag{34}$$

$$d(k_x, \omega) = k_x^2 + q^{*2}, \tag{35}$$

$$e(k_x) = k_x^2 + k_0^2. \tag{36}$$

Similarly, inhibitory power is given by

$$P_i(k_x, \omega) = \int_{-\infty}^{\infty} |\phi_i(\mathbf{k}, \omega)|^2 F(\mathbf{k}) dk_y. \tag{37}$$

The integral in Eq. (37) is calculated numerically in what follows, since its analytic form is too complicated to yield useful insight into its properties.

C. Further considerations

There are two further considerations. First, we note that experimentally measured potentials are not separable into excitatory and inhibitory components, but are more likely a linear combination of the fields of the two neuron populations [31]. Measured power is then given by

$$P(k_x, \omega) = \int_{-\infty}^{\infty} |W_e \phi_e + W_i \phi_i|^2 F(\mathbf{k}) dk_y \tag{38}$$

$$= W_e^2 P_e + W_i^2 P_i + 2 W_e W_i P_{ei}, \tag{39}$$

where the W_a represent the relative numbers of each type of neuron in the cortex, weighted by structural and orientation factors that affect their ability to generate observable potentials. The W_a are assumed here to be independent of ω and $\mathbf{k}$. The quantities P_e and P_i are derived above, and the quantity P_{ei} is incorporated numerically into the formulation of the scalp power spectra using

$$P_{ei}(k_x, \omega) = \mathrm{Re} \int_{-\infty}^{\infty} \phi_e(\mathbf{k}, \omega) \phi_i^*(\mathbf{k}, \omega) F(\mathbf{k}, \omega) dk_y. \tag{40}$$

Second, we note that the form of the equations derived allows the investigation of the wave-number spectrum for a single fixed ω. In experiments, however, it is a frequency band that is observed. Thus, in order to obtain a theoretical prediction which is comparable to the data, we need to integrate the predicted spectrum over a corresponding band:

$$P(k_x, \omega_1, \omega_2) = \int_{\omega_1}^{\omega_2} P(k_x, \omega) d\omega. \tag{41}$$

Unfortunately Eq. (41) cannot be evaluated analytically because of the complicated frequency dependence of q, so all integrals over frequency are calculated numerically below.

IV. EEG SPECTRA

In this section the 1D spatial spectrum derived from the model is discussed and illustrated, and parameter and frequency dependencies are investigated.

A. The spectrum

The form of the wave-number power spectrum was derived from the model in Sec. III. Figure 2 shows the resulting spectrum on the the scalp, i.e., including the effects of volume conduction. The parameters used are those given in Table I for the awake eyes-closed condition, and the spectrum is integrated over the frequency range 0.5–40 Hz.

Four curves are shown in Fig. 2, representing the weighted power contributions $W_e^2 P_e$, $W_i^2 P_i$, $2 W_e W_i P_{ei}$, and their sum P. The sum P represents the observed power, and in order to better understand it we qualitatively examine its components P_e, P_i, and P_{ei}. We begin with the quantity P_e. Ignoring the effects of volume conduction for the time
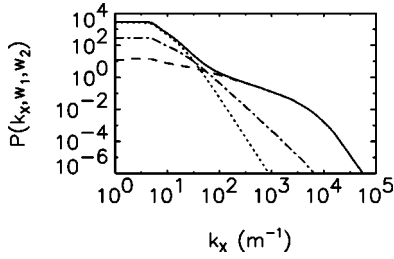
FIG. 2. Wave-number power spectrum from Eq. (38) derived from the model (solid line), for 0.5 Hz$<f<$40 Hz. Also shown are the contributions from the excitatory power $W_e^2 P_e$ (dotted line), the inhibitory power $W_i^2 P_i$ (dashed line), and the power $2W_e W_i P_{ei}$ (dot-dashed line). Parameters for all curves are given in Table I.

being, we concentrate on those factors in Eq. (13) that depend on k_x:

$$P_e(k_x, \omega) \propto \int_{-\infty}^{\infty} \frac{dk_y}{|k^2 + q^2|^2}. \qquad (42)$$

We see qualitatively that for $k_x \ll |q|$, P_e is constant, and for $k_x \gg |q|$, P_e decreases according to a power law. The transition between these two behaviors occurs at $k_x \approx |q|$, and for convenience shall be termed the excitatory knee. It is therefore the parameters in q^2 which dictate the position of this knee.

The precise nature of the power-law decrease for $k_x \gtrsim |q|$ is derived as follows: rewrite the k_x-containing factor in Eq. (14) as

$$P_e(k_x) = \frac{\text{Im}[\sqrt{q^2 + k_x^2}]}{\text{Im}(q^2)|q^2 + k_x^2|}. \qquad (43)$$

TABLE I. Parameters used in the model for each of the arousal states investigated. The parameters were chosen based on both physiological considerations and previous work using this model, as discussed in Sec. VI.

Parameter	Eyes closed	Eyes open	Sleep	Unit
t_0	0.07	0.07	0.07	s
r_e	0.08	0.08	0.08	m
r_i	0.0001	0.0001	0.0001	m
γ_i	10^5	10^5	10^5	s^{-1}
γ_e	200	180	100	s^{-1}
$\alpha = \beta/4$	40	75	50	s^{-1}
$G_{es} = G_{is}$	3.9	1.0	5.3	
G_{se}	2.6	1.0	0.1	
G_{sr}	-3.0	-1.0	-0.1	
G_{rs}	0.6	-0.1	7.0	
G_{ee}	6.2	4.0	6.0	
G_{ii}	-10	-3.4	-5.0	
G_{re}	0.3	0.5	5.1	
G_{sn}	5.0	2.8	0.2	
$W_e = 1 - W_i$	0.95	0.93–0.97	0.95	
k_0	25	25	25	m^{-1}

Now, for large k_x,

$$\text{Im}[\sqrt{q^2 + k_x^2}] \simeq \text{Im}\left[k_x\left(1 + \frac{q^2}{2k_x^2}\right)\right] \simeq \frac{\text{Im}(q^2)}{2k_x}, \qquad (44)$$

giving

$$P_e(k_x) \propto \frac{1}{\text{Im}(q^2)} \frac{\text{Im}(q^2)}{k_x^3} = k_x^{-3}. \qquad (45)$$

Consider now the effects of volume conduction. The filter function $F(\mathbf{k})$, from Eq. (28), is approximately constant for $k_x \lesssim k_0$, and has a slope that quickly increases to -1 at $k_x \approx k_0$, and gradually increases from -1 to -2 over the range $k_0 \lesssim k_x \lesssim 5k_0$, and has a constant slope of -2 for $k_x \gtrsim 5k_0$.

Combining the above, we find that the slope of the excitatory spectrum P_e is 0 for $0 < k_x \lesssim |q|$, then quickly increases to -3, where it remains for $|q| \lesssim k_x \lesssim k_0$, and gradually increases from -4 to -5 over the range $k_0 \lesssim k_x \lesssim 5k_0$, and is constant at -5 for $k_x \gtrsim 5k_0$. This assumes that $k_0 > |q|$, which is true over the frequency ranges considered here. In the case $k_0 < |q|$, the slope of the excitatory spectrum P_e is 0 for $0 < k_x \lesssim k_0$, then quickly increases to -1 at $k_x \approx k_0$, gradually increases from -1 to < -2 for $k_0 \lesssim k_x \lesssim |q|$ and from > -4 to -5 for $|q| \lesssim k_x \lesssim 5k_0$, and is constant at -5 for $k_x \gtrsim 5k_0$. The second sequence of slope magnitudes is easily determined from the first, so we assume $k_0 > |q|$ in what follows.

We now turn our attention to the qualitative behavior of P_i. Equations (24)–(26) show that the k_x-dependent part of P_i is

$$P_i(k_x, \omega) \propto \int_{-\infty}^{\infty} \frac{dk_y}{|k^2 + q^2|^2 |k^2 + h^2|^2}. \qquad (46)$$

Following the analysis of P_e, we would expect constant P_i for low k_x, and a power-law decrease at higher k_x, with knees at wave numbers dictated by the magnitudes of q and h. From the curve P_i in Fig. 2, we see that the effect of the knee at $|q|$ is negligible compared to the corresponding effect on P_e. For $k_x \gtrsim |h|$, the form of P_i is k_x^{-3}, following from the analysis for P_e.

Including the effects of volume conduction, which are exactly the same as for P_e, we find that the slope of the curve P_i is 0 for $0 < k_x \lesssim k_0$, increases from -1 to -2 over the range $k_0 \lesssim k_x \lesssim |h|$, and is -5 for $k_x \gtrsim |h|$.

Next, we consider the quantity P_{ei}, which is intermediate in character between P_e and P_i. It retains the features of both these curves; i.e., has knees at each of $|q|$, k_0, and $|h|$, with the power-law exponent varying from zero at low k_x to -5 at $k_x \gtrsim |h|$.

Finally, we deduce the behavior of the measurable power P, which is simply the weighted sum of the above three quantities. As such, it is constant for low k_x ($k_x \lesssim |q|$) and k_x^{-5} for high k_x ($k_x \gtrsim |h|$). At intermediate values of k_x, the measured power simply follows the shape of whichever of P_e, P_i, or P_{ei} is dominant. There are many more excitatory neurons than inhibitory ones, and they are aligned to give a

stronger signal [41]. Thus P_e dominates at large scales (low k_x). The quantity P_e, however, is the first to diminish as k_x increases, hence domination switches to P_i at some point, which we designate k_{ei}. The value of k_{ei} primarily depends on W_e, r_e, and the frequency-dependent factors in P_e and P_i.

Combining all the above considerations, we find that the spectral power decreases with wave number according to the power law

$$P(k_x, \omega_1, \omega_2) \propto k_x^{-g}, \tag{47}$$

with $g \approx 0$ for $0 \lesssim k_x \lesssim |q|$, $0 \leq g \leq 3$ for $|q| \lesssim k_x \lesssim k_0$, $1 \leq g \lesssim 5$ for $k_0 \lesssim k_x \lesssim k_{ei}$, $1 \leq g \leq 2$ for $k_{ei} \lesssim k_x \lesssim |h|$, and $g \approx 5$ for $k_x \gtrsim |h|$.

The inequalities result from the fact that P is summed, and the value taken depends on the ratio W_e/W_i, and on ω_1 and ω_2, which we investigate more fully in Sec. V B. Note that the varying contribution from the head filter function $F(\mathbf{k})$ as k_x increases from below k_0 to above $5k_0$ has been included. The locations of the various knees can be roughly approximated as $|q| \approx 1/r_e \approx 10$ m^{-1}, $k_0 \approx 25$ m^{-1} [24,40], $k_{ei} \approx 50$ m^{-1}, $|h| \approx 1/r_i \approx 10^5$ m^{-1}. For the spectrum shown in Fig. 2, only four of the five zones are clearly distinguishable, with $g \approx 0$, 3, 2, 5, and only a slight hump at $k_0 = 25$ m^{-1}.

To relate these results to experiments, one must remember that $k_x < 7$ m^{-1} on the cortex corresponds to scalp wavelengths larger than 60 cm, the approximate circumference of the head, and as such is not relevant in practice. (This estimate is calculated using a cortical folding parameter of 1.5 [24] to account for the convolutions in the cortex.) Also, $k_x > 10^4$ m^{-1} corresponds to cortical wavelengths smaller than 0.6 mm, which is approaching the limit of validity of the theory, since the model averages over scales smaller than a few tenths of a millimeter. Thus, it is primarily the region 7 m$^{-1} < k_x < 10^4$ m^{-1} that is of interest here.

B. Parameter sensitivities

In this section we examine how the spectrum varies with each of the model parameters, concentrating on those which most affect the index g as given in Eq. (47). The effects of r_e, γ_e, k_0, W_e, r_i, and G_{sn} are shown in Fig. 3, the others briefly discussed. In each frame, all parameters other then that being varied are fixed at the values in Table I, and possible correlations between changes in parameters are not considered. The reasons for each choice of parameter range are discussed in Sec. VI, and lie near the values in Table I.

We first investigate the parameters which affect the excitatory knee; i.e., those which significantly influence $|q|$. Figure 3(a) shows the effect of varying r_e from 5 cm to 10 cm. As r_e increases, $|q|$ decreases and the excitatory knee moves to lower k_x. Figure 3(b) shows the effect of varying γ_e from 150 s^{-1} to 250 s^{-1}. The knee moves to lower k_x as $|q|$ is decreased, and the power increases. The remaining parameters that appear in Eq. (10) are α, G_{ee}, G_{es}, and G_{ii}. These also affect the excitatory knee, either by a slight shift or by sharpening it; however, the effects are minimal since q
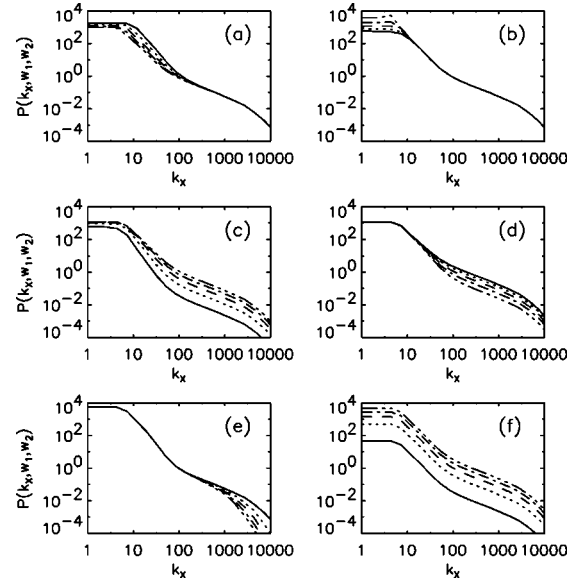
FIG. 3. Dependences of the power spectrum on individual parameters for the frequency range 0.5 Hz $< f <$ 40 Hz, with other parameters fixed at the values in Table I. Solid, dotted, dashed, dotdashed curves are used in order of increasing magnitude of the parameter being varied. Values are (a) 5 cm $< r_e <$ 10 cm, (b) 150 s$^{-1} < \gamma_e < 250$ s^{-1}, (c) 5 m$^{-1} < k_0 <$ 30 m^{-1}, (d) $0.92 < W_e < 0.97$, (e) 0.1 mm $< r_i <$ 0.5 mm, and (f) $1 < G_{sn} < 10$.

is relatively weakly dependent on them, except at sharp spectral resonances, which are integrated over in any case. Two of them, G_{es} and G_{ii}, also affect the power at all k_x due to their contribution to the k_x-independent prefactors in both P_e and P_i.

We next examine the spectral dependence on the head filter function. The quantity k_0 is varied from 5 m^{-1} to 30 m^{-1} in Fig. 3(c), the approximate range of values deduced from the work of Srinivasan *et al.* [40]. As k_0 increases, the onset of the additional filtering is shifted to higher k_x, and the overall slope of the region 10 m$^{-1} < k_x < 100$ m^{-1} decreases.

Figure 3(d) shows the effect of varying W_e from 0.92 to 0.97, which affects k_{ei}. Indeed, as W_e increases, the transition from high to low g at around 100 m^{-1} shifts to higher k_x, with no transition at all in the limit $W_e = 1$.

Figure 3(e) shows the effect of varying r_i from 0.1 mm to 0.5 mm, which decreases $|h|$ and consequently moves the inhibitory knee to lower k_x.

The gain G_{sn} represents input to the thalamus from subthalamic regions, and is increased from 1 to 10 in Fig. 3(f). As external input to the system G_{sn} is increased, overall power is increased. This is reflected mathematically in the fact that G_{sn} appears only in the k_x-independent factors in P_e, P_i, and P_{ei}.

The remaining model parameters, G_{re}, G_{se}, G_{sr}, G_{rs}, and t_0, have only minor effects on the spectrum, particularly in the range of interest 7 m$^{-1} < k_x < 10^4$ m^{-1}.

C. Spatiotemporal relationships

We now turn our attention to the interplay of spatial and temporal frequencies in the brain. The existence of a rela-
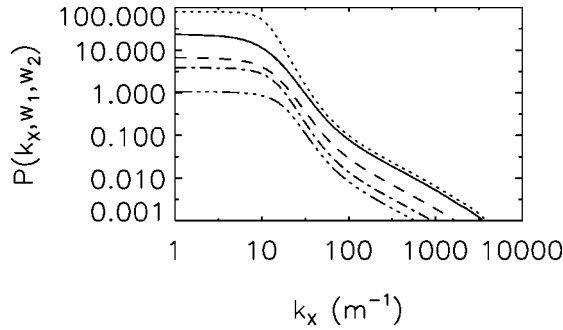
FIG. 4. Spatial spectra at 5 Hz (solid), 10 Hz (dotted), 15 Hz (dashed), 20 Hz (dot-dashed), and 25 Hz (triple dot-dashed), using the parameters in Table I. There is a general trend to decreasing total power with increasing frequency; however the trend is not monotonic since the curve at 10 Hz lies above that at 5 Hz.

tionship between the two is verified by inspection of Fig. 4, which shows the theoretical spatial spectrum (38) at the five frequencies 5 Hz, 10 Hz, 15 Hz, 20 Hz, 25 Hz. Parameters are for the eyes-closed state, given in Table I.

We first note that the qualitative form of the spectrum is the same over the f bands; i.e., there is always a low-k_x plateau followed by a number of roughly power-law decreases in $P(k_x,\omega)$ with varying exponents, as discussed in relation to Fig. 2. There is also a general trend to decreasing power with increasing frequency; however the decrease is not monotonic since the spectrum at 10 Hz lies above that at 5 Hz. In fact, the total power fluctuates with frequency in the same way as the temporal frequency power spectrum. That is, for the eyes-closed case, maximums in power occur at multiples of the resonant alpha frequency at 10 Hz, superimposed on a background of decreasing power with increasing frequency. Indeed, in the eyes-open case (not shown) the power maximum at the alpha frequency is greatly diminished, and in sleep (also not shown) the maximums are shifted to ≈ 5 Hz, 15 Hz, etc., corresponding to theta and spindle peaks in the sleep frequency power spectrum [42]. The background of decreasing power is related to the action of the dendrites as low-pass temporal frequency filters, and is minimized by increasing the parameter α.

We have established that the spatial power spectrum depends on frequency, and in fact low k_x and low ω are correlated via the wave dipersion relation. We now investigate the f dependence of the region of power-law decrease in P which starts at the excitatory knee. Ignoring volume conduction for the time being, the cortical power P_e is given by Eq. (14), with k_x dependence given by

$$P_e(k_x,\omega) \propto 1/[\mathrm{Re}(\sqrt{q^2+k_x^2})|q^2+k_x^2|]. \qquad (48)$$

The derivative of $P_e(k_x,\omega)$ with respect to k_x is of the form

$$\frac{dP_e}{dk_x} \propto \frac{-k_x}{|k_x^2+q^2|^n}, \qquad (49)$$

which decreases in magnitude with increasing $|q|$ for a given k_x. Including volume conduction simply adds a frequency
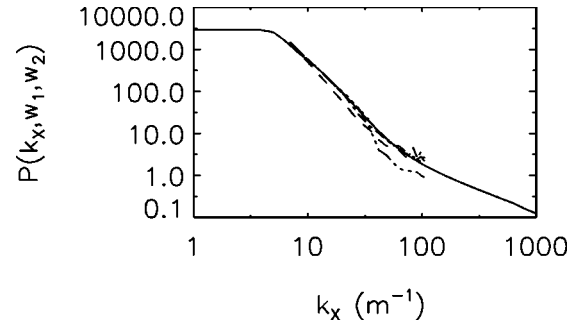
FIG. 5. Wave-number power spectrum for awake, eyes closed, for 0.5 Hz$<f<$40 Hz. The theoretical spectrum derived from the model, using parameters for eyes closed in Table I (solid line), and scalp data recorded by Shaw from four subjects awake, eyes closed (broken lines).

independent factor of about 2. Thus, we expect the slope of the spatial spectrum in the region $|q|<k_x<k_{ei}$ to be greatest for small values of $|q|$.

Previous work using this model has shown that small values of $|q|$ correspond to peaks in the frequency spectrum [29]. We would therefore expect the slope of the wave-number spectrum to have maximums at the frequencies of peaks in the frequency spectrum.

A more detailed exploration of the frequency dependence of the power-law exponent g is defered to the following section, where it is compared with experimental data from a different study.

V. COMPARISON WITH EEG DATA

In this section the theoretical scalp wave-number spectrum is compared with data obtained from recordings by Shaw [22], for both the awake eyes-closed and awake eyes-open conditions. The predicted spectrum for slow-wave sleep is also presented, although we could find no published data for comparison. The model parameters used for each of the various states are listed in Table I.

A. EEG spectrum

Shaw [22] used a circular 1D montage of 31 equally spaced electrodes placed around the head in a horizontal plane passing just above the ears, to record the EEG wave-number spectra of four subjects, with a single reference electrode on the crown of the head. Shaw removed the effects of the active reference electrode on the recorded signal by subtracting the spatial average from the data. The array circumference was ≈ 60 cm, with interelectrode spacing of ≈ 2 cm, giving a wave-number range 7 m$^{-1}<k_x<$100 m^{-1}, incorporating a cortical folding parameter of 1.5 [24], and using the Nyquist wave number as the upper bound. Recordings were made from the subjects in both the awake eyes-closed and awake eyes-open conditions.

Both theoretical and experimental spectra are shown in Figs. 5 and 6 for the eyes-closed and eyes-open conditions, respectively, with parameters for the theoretical curves given in Table I. Both theoretical and experimental spectra have f $=0.5$–40 Hz.
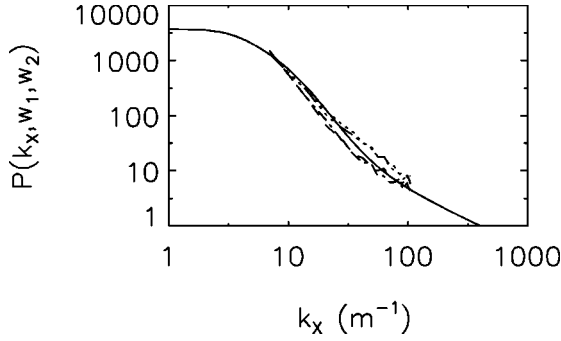
FIG. 6. Wave-number power spectrum for awake, eyes open, for 0.5 Hz$<f<40$ Hz. The theoretical spectrum derived from the model, using parameters for eyes open in Table I (solid line), and scalp data recorded by Shaw from four subjects awake, eyes open (broken lines).

For the eyes-closed spectra in Fig. 5, there is good qualitative agreement between theory and data. Shaw noted that the power-law relationship (47) holds, and calculated the average experimental exponent in the range 7 m$^{-1}<k_x<42$ m^{-1} to be $g=3.0\pm0.4$ [22]. A theoretical value of $g=2.7\pm0.5$ was calculated using linear regression over the same range, where the estimated error includes uncertainties due to varying the range of the linear regression.

The eyes-open spectrum, seen in Fig. 6, is very similar to the eyes-closed one, but has a slightly shallower slope. There is also good agreement between experiment and theory. Shaw found a mean power-law exponent of $g=2.3\pm0.3$, which agrees well with the theoretical value of $g=2.3\pm0.3$ over the same k_x range.

For both eyes closed and eyes open, Shaw assumed the exponent g in Eq. (47) to be constant for all $k_x>0$; however he recognized the reduced slope of the spectra at larger k_x (>40 m^{-1}) and attributed this to experimental error, citing as possible sources spatial aliasing, noise, and imprecision in electrode placement. Our model suggests that the reduction in slope is a real phenomenon, occurring as the power in the inhibitory neuron population becomes larger than the rapidly diminishing excitatory neuronal power. For the data above 40 m^{-1}, Shaw did not calculate the slope of the spectrum. A linear regression analysis of this data in the range 42 m$^{-1}<k_x<100$ m^{-1} gives $g\approx1.5$ for both eyes closed and open, which falls within the theoretical range of g from Eq. (47) for the corresponding wave numbers $k_{ei}<k_x<|h|$.

If we removed the effects of volume conduction to examine cortical power, the slopes of the spectra above $k_0\approx25$ m^{-1} would be reduced, with the greatest effect for $k_x>5k_0$. That is, the portion of the spectra at $5k_0<k_x<|h|$ would be flattened to a plateau, and the slope at $k_x>|h|$ would be reduced from $g=5$ to $g=3$.

B. Frequency dependence of g

For the eyes-closed state, Fig. 7 shows both the theoretical and experimental slopes. The parameters used in derivation of the theoretical curve, given in Table I, are the same as those used for comparison with the same four subjects' power spectra in Fig. 5. From the theory, the value of g was
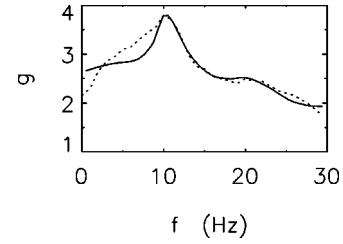
FIG. 7. Dependence of the power-law index g on frequency f for the awake, eyes-closed condition. Theoretical results are obtained using parameters from Table I (solid line), and mean experimental results are from four subjects (broken line). The index g is greatest at multiples of the alpha frequency of 10 Hz, and decreases with increasing frequency.

again calculated using linear regression, with a fixed end point at $k_x\approx40$ m^{-1}. The start point, however, was allowed to vary to reflect the fact that the onset of the power-law decrease is itself a function of frequency. The onset was taken to be the point at which the instantaneous slope was halfway between the value at $k_x=0$ and at $k_x=40$ m^{-1}. Comparing the theoretical results with the data, we see that there is good agreement: first, g has maximums at multiples of the resonant alpha frequency, and second, there is a trend to smaller g with increasing frequency. Below 8 Hz there is a narrowing of the theoretical peak relative to the experimental one. A possible source of this discrepancy is an experimentally introduced error due to increasing phase differences between recording channels as the lower cutoff frequency of the analog band-pass filters is approached, as discussed by Shaw [22]. The channels' low-frequency responses were not corrected for this effect [22], however we would not expect it to influence the signal at frequencies as large as 8 Hz.

We next examine the work of Wingeier *et al.* who implemented a spherical harmonic analysis of awake, eyes-closed EEG from six subjects [23]. They plotted the ratio of the power in low wave numbers to power in high wave numbers, which acts as an approximate measure of the slope. Power ratio was plotted against temporal frequency at 1 Hz resolution, and the results are shown in Fig. 8(a). Figure 8(b) shows the theoretical curve from Fig. 7. The Wingeier results agree qualitatively with those reported by Shaw [22] and those presented here. That is, the power ratio is greatest at the alpha frequency 10 Hz, with a possible second peak at 20 Hz, and an overall decrease with increasing frequency. We see that the width of the peak at 10 Hz varies with each individual.

Further experimental evidence for a maximum in g at around 10 Hz is provided by Nunez [24,43]. Nunez recorded 2D EEG data which yielded an approximate range $g=3-5$ for frequencies at 8.0 Hz and 9.5 Hz, indicating a g value at these frequencies which was elevated from the base value of $g=2-3$. These ranges of g correspond closely with the theoretical ranges for $|q|<k_x<k_{ei}$, Eq. (47).

We now turn our attention to the results for eyes-open EEGs. Figure 9 shows both the theoretical and experimental [24] power-law exponents for eyes open. The parameters used in derivation of the theoretical curve are the same as those used for comparison with the same four subjects'
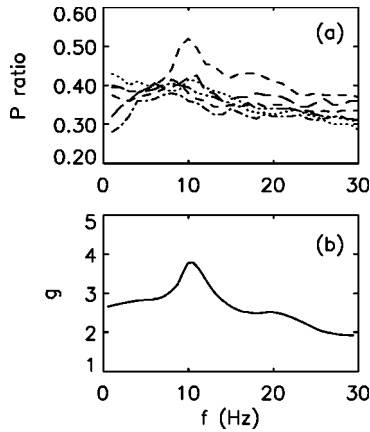
FIG. 8. Frame (a) shows the frequency dependence of the ratio of power in low wave numbers to power in high wave numbers, recorded by Wingeier *et al.* from six eyes-closed subjects. The experimental ratios give a crude approximation to the exponent g. Frame (b) shows the theoretical dependence of g on f for the awake, eyes-closed state, the same curve as in Fig. 7.

power spectra in Fig. 6. Comparing the theoretical results with the data, the match is less convincing than for the eyes-closed state, however we do find good agreement, especially for $f > 5$ Hz. The divergence between theory and data below 5 Hz may be explained by low-f experimental error, as discussed in relation to the eyes-closed case. The divergence between the curves at $f > 25$ Hz may indicate that the form of the head filter function in Eq. (28) needs to be adjusted. Alternatively, the experimental g may be artifically lowered by not accounting for the varying onset of the power-law decreases; e.g., the value could incorporate both the legitimate decrease in power and a portion of the low-k_x power plateau. There is a possible indication of a similar effect between theory and data above 28 Hz for the eyes-closed case. More experiments need to be done in order to distinguish between these two possibilities.

We remark that the peak in g at the alpha frequency is lower and flatter than for the eyes-closed condition. Mathematically, this results from the larger values of $|q|$ in this case due to the different parametrization. Physiologically, this reflects the diminishment of the alpha rhythm in the eyes-open EEG.

The theory is not limited to eyes-closed and eyes-open waking states, and we now extend it to explore a sleeping
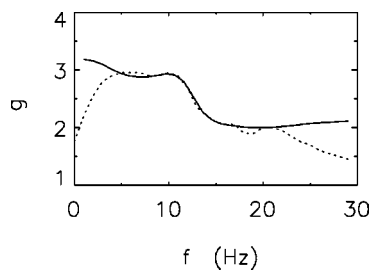
FIG. 9. Dependence of the power-law index g on frequency f for the awake, eyes-open condition. Theoretical results are obtained using parameters from Table I (solid line), and the mean experimental results are from four subjects (broken line).
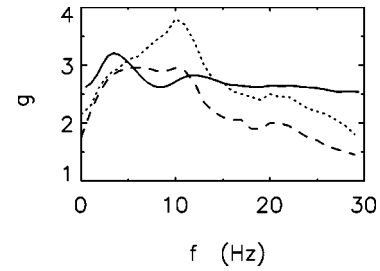
FIG. 10. Predicted dependence of the exponent g on frequency f for slow-wave sleep. Theoretical results are produced using parameters from Table I (solid line). Also shown are experimental data for awake eyes closed (dotted line) and awake eyes open (dashed line). Peaks shift towards θ and spindle frequencies, which dominate in sleep.

state. We could not find any data in the literature for spatial EEG spectra of sleeping subjects, and so use the theory presented here to predict the form of this spectrum, in particular, its dependence on f. Predicted spectral slope variation for slow-wave sleep is shown in Fig. 10, overplotted with the data for awake, eyes closed and awake, eyes open.

Recall that peaks of g should occur at frequencies which correspond to peaks in the temporal frequency power spectrum. For the predicted sleep curve, peaks in g occur between peaks in the awake curves, at about 3 Hz and 12 Hz, i.e., at theta and spindle frequencies, which dominate in slow-wave sleep [29,42].

VI. PARAMETER CHOICE AND EXTRACTION

The parameters used in generation of the theoretical curves are given in Table I. We now discuss the validity of the particular values chosen, and their relative magnitudes in the different brain states. The parameters in the top section of the table do not vary between states; the range parameters represent the physical extent of the neurons, and there is no evidence for these changing dynamically. The corticothalamic loop time t_0 and inhibitory damping γ_i have been set as constants because of the lack of evidence to the contrary. Indeed, both the spectrum and exponent g are insensitive to changes in γ_i until it is decreased by four or five orders of magnitude. The loop time t_0 should be approximately constant, however it may change under halothane anesthesia [24], and future experimental work using this drug could provide a test of the model.

The middle section of the table shows those parameters which vary between states. These reflect values and changes which have been independently determined using this model in the time domain [34], and by physiological considerations. For example, fitting the model to EEG data obtained from 100 subjects with eyes closed and open showed a statistically significant decrease in the excitatory damping parameter γ_e for eyes open compared to eyes closed [34]. Similarly, there was a significant increase in α, and significant decreases in the composite quantities $G_{es}G_{se}$ and $G_{sr}G_{rs}$. These trends, which are reflected in Table I, were also independently reproduced by EEG simulation in the time domain using this model [32]. This simulation also indicated that G_{ee} and G_{ii}

are reduced in magnitude for eyes-open EEG, and that G_{re} and G_{sn} are increased.

The actual values taken by various parameters lie within the range determined by both the EEG fits and the simulation. Certain combinations of these parameters, termed x,y,z, have been shown to be robust measures of the brain state [32], where $x=G_{ee}/(1-G_{ii})$ provides a measure of cortical activity, $y=(G_{es}G_{se}+G_{es}G_{sr}G_{re})/[(1-G_{sr}G_{rs})(1-G_{ii})]$ provides a measure of corticothalamic activity, and $z=-\alpha\beta G_{sr}G_{rs}/(\alpha+\beta)^2$ provides a measure of thalamic activity. For eyes closed and eyes open, respectively, from Table I, we have $x=0.56,0.91$, $y=0.22,0.13$, $z=0.29$, -0.02, which corresponds well with other studies [32,34]. For the sleep curves, the parameter values were taken directly from a slow-wave sleep simulation, with $x=1.00$, $y=-0.27$, and $z=0.16$.

The bottom section of the graph shows those parameters which could not be well constrained by other considerations, namely, the head filter constant k_0, and the relative contribution of the excitatory population W_e, where we have taken $W_e+W_i=1$ for convenience. The parameter k_0 was limited by consideration of the head volume conductor model developed by Srinivasan *et al.* [40] and the contribution of the excitatory population is known to greatly exceed that of the inhibitory population. The present study, however, allows us to more precisely extract these parameters by fitting the theory to the data, with the other model parameters constrained as discussed above. We conclude that the head filters out wave numbers above $k_x\approx25$ m^{-1}, which is consistent with the model results of Srinivasan *et al.* Also, the excitatory neurons contribute $\approx95\%$ of the measured signal due to their higher prevalence, their structure, and their aligned orientation.

VII. SUMMARY AND DISCUSSION

We have used our existing neurophysical continuum model of brain dynamics to explore the EEG power spectrum in the spatial domain. We argue that this has two main benefits: insight into the spatial activity of the brain from a new perspective, and the extension and validation of the model. We discuss each of these in turn.

The scalp wave-number spectrum was found to consist of a low-k_x plateau followed by a power-law monotonic decrease of the form $P=k_x^{-g}$, where g depends on both k_x and ω. The k_x dependence of g offers insight into which neural populations and brain parameters dominate the activity at different scales. At large scales ($k_x\lesssim|q|$), excitatory contributions to measured power dominate because of the prevalence of excitatory neurons, and their structure and alignment. At slightly smaller scales ($k_x\gtrsim|q|$), their dominance diminishes. For still smaller scales ($k_x\gtrsim k_0$), scalp power is further reduced by the filtering out of small-scale activity by the cerebrospinal fluid, skull, and scalp. At even smaller scales ($k_x\gtrsim k_{ei}$), the excitatory power is so diminished that the power in the inhibitory population dominates. This in turn is reduced at scales approaching that of the inhibitory neural range r_i ($k_x\gtrsim|h|$). For smaller scales than this the continuum approach is no longer valid.

A fuller parameter investigation indicated those parameters which most affect the spectrum. These include the range, feedback, and head filtering parameters, and the relative contributions of the two neural populations. An important outcome of this analysis is an estimation of those parameters which are otherwise ill constrained; in particular, the wave numbers which are filtered out by the head, and the relative contributions of the two populations to observed scalp power.

The existence of a power-law decrease in power for the range 7 m$^{-1}<k_x<40$ m^{-1} was confirmed by experimental data collected by Shaw [22], and the value of g was in agreement for both eyes closed and open. To verify the theoretical predictions at smaller scales, experiments with smaller interelectrode distances need to be performed.

As stated above, the exponent g also depends on temporal frequency ω, with maximums in g coinciding with peaks in the frequency power spectrum. An analysis of this frequency dependence for the range 7 m$^{-1}<k_x<40$ m^{-1} and 0.5 Hz $<f<30$ Hz yielded good agreement with Shaw's data for both eyes closed and open. The exponent also agreed with data collected by Nunez [24]. For eyes closed, the slope had a large maximum at the alpha frequency, 10 Hz. This peak was much diminished in the eyes-open spectrum, which reflects the phenomenon of alpha blocking in the temporal domain. Also, increasing frequency led to a decrease in total power, which relates the established temporal mechanism of dendritic low-pass filtering to the spatial domain, underlining the link between spatial and temporal activity and establishing the relevance of understanding the wave-number behavior of the brain.

The frequency dependence of the exponent g for slow-wave sleep was predicted, with maximums shifted to frequencies corresponding to theta and spindle spikes, which are known to occur in slow-wave sleep. In order to confirm these predictions, relevant experimental data are required.

Let us consider now the model itself. It has been used previously to accurately model the temporal power spectrum for a variety of brain states. The relative wealth of data available in the temporal domain has provided ample validation of the theory. Here, we have shown that the same model can be used in the spatial domain. The parameters used for the different states were taken from previous studies, and shown to produce results which fit the data. We have confirmed that changes in brain state, such as eyes-open, -closed, or sleep, can be modeled by a simple change of parameters, a fact which underlines the unity of brain function. That is, different states of arousal are simply attributed to a change in thalamocortical gains, and their description can be unified into a single theory such as that explored here, rather than the approach typically used in the past whereby different aspects of cortical activity were explained by quite different models.

The version of the model used here is infinite, and thus ignores any possible contribution to the spectrum by cortical boundary conditions. Boundary conditions have been shown previously to have very minor effects on the cortical dynamics produced by this model under most circumstances, with the exception being for weak cortical damping. In any case,

finite model dynamics would be expected to differ from infinite ones only at the largest scales, so the bulk of the spectrum would remain unchanged. A possible extension of this work would be to investigate these large-scale effects.

In conclusion, the spatial spectrum has been theoretically derived and shown to reflect activity in the temporal frequency domain. The results have been shown to agree with the available data, although such data are limited and further experiments with extended frequency and wave-number ranges are needed. The wave-number analysis could be generalized to two-dimensional spectra, rather than their one-dimensional projections, thereby allowing comparison with data obtained from 2D electrode arrays. The 1D wave-number analysis has been integrated into an existing framework which describes and explains many disparate aspects of brain behavior.

ACKNOWLEDGMENTS

APPENDIX: EVALUATION OF INTEGRALS IN DERIVATION OF CORTICAL P_i

The integrals (24)–(26) can be evaluated using the relation $|z|^2 = zz^*$ for complex z. This gives

$$I_1(\mathbf{k}, \omega) = \int_{-\infty}^{\infty} \frac{k_y^4 dk_y}{(k_y^2 + c)(k_y^2 + d)(k_y^2 + m)(k_y^2 + n)}$$

$$= \pi \left[-c^2 \sqrt{\frac{1}{c}}(c-d)^{-1}(c-m)^{-1}(c-n)^{-1} \right.$$

$$+ d^2 \sqrt{\frac{1}{d}}(c-d)^{-1}(d-m)^{-1}(d-n)^{-1}$$

$$- m^2 \sqrt{\frac{1}{m}}(c-m)^{-1}(d-m)^{-1}(m-n)^{-1}$$

$$\left. + n^2 \sqrt{\frac{1}{n}}(c-n)^{-1}(d-n)^{-1}(m-n)^{-1} \right],$$

$$\tag{A1}$$

$$I_2(\mathbf{k}, \omega) = \int_{-\infty}^{\infty} \frac{k_y^2 dk_y}{(k_y^2 + c)(k_y^2 + d)(k_y^2 + m)(k_y^2 + n)}$$

$$= \pi \left[c \sqrt{\frac{1}{c}}(c-d)^{-1}(c-m)^{-1}(c-n)^{-1} \right.$$

$$- d \sqrt{\frac{1}{d}}(c-d)^{-1}(d-m)^{-1}(d-n)^{-1}$$

$$+ m \sqrt{\frac{1}{m}}(c-m)^{-1}(d-m)^{-1}(m-n)^{-1}$$

$$\left. - n \sqrt{\frac{1}{n}}(c-n)^{-1}(d-n)^{-1}(m-n)^{-1} \right],$$

$$\tag{A2}$$

$$I_3(\mathbf{k}, \omega) = \int_{-\infty}^{\infty} \frac{dk_y}{(k_y^2 + c)(k_y^2 + d)(k_y^2 + m)(k_y^2 + n)}$$

$$= \pi \left[- \sqrt{\frac{1}{c}}(c-d)^{-1}(c-m)^{-1}(c-n)^{-1} \right.$$

$$+ \sqrt{\frac{1}{d}}(c-d)^{-1}(d-m)^{-1}(d-n)^{-1}$$

$$- \sqrt{\frac{1}{m}}(c-m)^{-1}(d-m)^{-1}(m-n)^{-1}$$

$$\left. + \sqrt{\frac{1}{n}}(c-n)^{-1}(d-n)^{-1}(m-n)^{-1} \right], \tag{A3}$$

with

$$c = k_x^2 + q^2, \tag{A4}$$

$$d = k_x^2 + q^{*2}, \tag{A5}$$

$$m = k_x^2 + h^2, \tag{A6}$$

$$n = k_x^2 + h^{*2}. \tag{A7}$$

[1] M.C. Steriade, D.A. McCormick, and T.J. Sejnowski, Science **262**, 679 (1993).

[2] R.R. Llinás and D. Paré, Neuroscience **44**, 521 (1991).

[3] M. Schoppenhorst, F. Brauer, G. Freund, and St. Kubicki, Electroencephalogr. Clin. Neurophysiol. **48**, 25 (1980).

[4] E. Niedermeyer, Int. J. Psychophysiol **26**, 31 (1997).

[5] F. Aoki, E.E. Fetz, L. Shupe, E. Lettich, and G.A. Opejman, J. Clin. Neurophysiol. **110**, 524 (1999).

[6] A.W. de Weerd, W.V.M. Perquin, and E.J. Jonkman, Dementia **1**, 115 (1990).

[7] M.Y. Neufeld, S. Blumen, I. Aitkin, Y. Parmet, and A.D. Korczyn, Dementia **5**, 23 (1994).

[8] A. Stevens and T. Kircher, Eur. Arch. Psychiatry Clin. Neurosci. **248**, 259 (1998).

[9] H. Tanaka, T. Koenig, R.D. Pascual-Marqui, K. Hirata, K. Kochi, and D. Lehmann, Dement Geriatr. Cogn Disord. **11**, 39 (2000).

[10] L. Pezard, R. Jech, and E. Ružička, J. Clin. Neurophysiol. **112**, 38 (2001).

[11] W.J. Freeman, Electroencephalogr. Clin. Neurophysiol. **44**, 586 (1978).

[12] W.J. Freeman and B.W. van Dijk, Brain Res. **422**, 267 (1987).

[13] N.E. Crone, D.L. Miglioretti, B. Gordon, J.M. Sieracki, M.T. Wilson, S. Uematsu, and R.P. Lesser, Brain **121**, 2271 (1998).

[14] V. Menon, W. Freeman, B.A. Cutillo, J.E. Desmond, M.F. Ward, S.L. Bressler, K.D. Laxer, N. Barbaro, and A.S. Gevins, Electroencephalogr. Clin. Neurophysiol. **98**, 89 (1996).

[15] P.L. Nunez, B.M. Wingeier, and R.B. Silberstein, Hum. Brain Mapp **13**, 125 (2001).

[16] E. Niedermeyer and F.H. Lopes da Silva, *Electroencephalography: Basic Principles, Clinical Applications, and Related Fields*, 4th ed. (Williams and Wilkins, Baltimore, 1999).

[17] B. Shen, M. Nadkarni, and R.A. Zappulla, J. Clin. Neurophysiol. **110**, 115 (1999).

[18] A.S. Gevins, P. Brickett, B. Costales, J. Le, and B. Reutter, Brain Topogr **3**, 53 (1990).

[19] L.J. Pinson and D.G. Childers, IEEE Trans. Biomed. Eng. **21**, 3 (1974).

[20] P.L. Nunez, IEEE Trans. Biomed. Eng. **21**, 473 (1974).

[21] W.J. Freeman, L.J. Rogers, M.D. Holmes, and D.L. Silbergeld, J. Neurosci. Methods **95**, 111 (2000).

[22] G.R. Shaw, Ph.D. dissertation, University of Alberta, Alberta, Canada, 1991 (unpublished).

[23] B.M. Wingeier, P.L. Nunez, and R.B. Silberstein, Phys. Rev. E **64**, 051916 (2001).

[24] P.L. Nunez, *Neocortical Dynamics and Human EEG Rhythms* (Oxford, Oxford, 1995).

[25] P.A. Robinson, C.J. Rennie, and J.J. Wright, Phys. Rev. E **56**, 826 (1997).

[26] P.A. Robinson, J.J. Wright, and C.J. Rennie, Phys. Rev. E **57**, 4578 (1998).

[27] P.A. Robinson, C.J. Rennie, J.J. Wright, and P.D. Bourke, Phys. Rev. E **58**, 3557 (1998).

[28] C.J. Rennie, P.A. Robinson, and J.J. Wright, Phys. Rev. E **59**, 3320 (1999).

[29] P.A. Robinson, C.J. Rennie, J.J. Wright, H. Bahramali, E. Gordon, and D.L. Rowe, Phys. Rev. E **63**, 021903 (2001).

[30] P.A. Robinson, P.N. Loxley, S.C. O'Connor, and C.J. Rennie, Phys. Rev. E **63**, 041909 (2001).

[31] C.J. Rennie, P.A. Robinson, and J.J. Wright, Biol. Cybern. **86**, 457 (2002).

[32] P.A. Robinson, C.J. Rennie, D.L. Rowe, and R.C. Powles, Phys. Rev. E **65**, 041924 (2002).

[33] P.A. Robinson (unpublished).

[34] D.L. Rowe, P.A. Robinson, and C.J. Rennie (unpublished).

[35] F.H. Lopes da Silva, A. Hoeks, H. Smits, and L.H. Zetterberg, Kybernetik **15**, 27 (1974).

[36] M.C. Steriade, P. Gloor, R.R. Llinás, F.H. Lopes da Silva, and M.M. Mesulam, Electroencephalogr. Clin. Neurophysiol. **76**, 481 (1990).

[37] W.J. Freeman, Int. J. Bifurcation Chaos Appl. Sci. Eng. **2**, 451 (1992).

[38] J.J. Wright and D.T.J. Liley, Behav. Brain Sci. **19**, 285 (1996).

[39] E.G. Jones, *The Thalamus* (Plenum, New York, 1985).

[40] R. Srinivasan, P.L. Nunez, and R.B. Silberstein, IEEE Trans. Biomed. Eng. **45**, 814 (1998).

[41] D.T. Liley and J.J. Wright, Network Comput. Neural Syst. **5**, 175 (1994).

[42] M. Steriade, Neuroscience **101**, 243 (2000).

[43] P.L. Nunez, in *Statistics and Topography in Quantitative EEG*, edited by D. Samson-Dollfus (Elsevier, Paris, 1988).